J Appl Electrochem (2013) 43:1243–1248
DOI 10.1007/s10800-013-0612-8

RESEARCH ARTICLE

The study on the Li-storage performances of bamboo charcoal (BC) and BC/Li_2SnO_3 composites

Yang Zhao · Ying Huang · Qiufen Wang · Wei Zhang · Ke Wang · Meng Zong

Received: 29 May 2013 / Accepted: 8 August 2013 / Published online: 17 August 2013

Abstract Bamboo charcoal/Li_2SnO_3 composites for lithium-ion batteries were synthesized by a sol–gel route. The structure, morphology, and electrochemical properties of the composites were detected by means of X-ray diffraction, scanning electron microscope, Raman spectroscopy, thermal gravimetric analysis, and electrochemical measurements. The results showed that Li_2SnO_3 particles were loaded on the surface of bamboo charcoal and some of them entered into the hole. The bamboo charcoal/Li_2SnO_3 composites exhibited good electrochemical performance with high capacity and good cycling stability (616.5 mAh g^{-1} after 50 cycles). The composites showed a better electrochemical property than Li_2SnO_3 and bamboo charcoal.

Keywords Bamboo charcoal · BC/Li_2SnO_3 composites · Sol–gel method · Lithium-ion batteries · Electrochemical properties

1 Introduction

The lithium-ion battery is considered to be an excellent power source for portable electronic products and electric vehicle, because of its small size and high energy density. The development of new electrode materials is a key factor to improve the performance of lithium-ion battery. At present, graphite is widely used as an anode material for lithium-ion batteries, but its relatively low theoretical capacity (372 mAh g^{-1}) limits the further applications [1]. Among the many possible anodes, tin-based materials, such as $CdSnO_3$ [2], $CaSnO_3$ [3], Mg_2SnO_4 [4], $CoSnO_3$ [5], Sn–Cu [6], Sn–Sb–Cu [7], and SnO_2 [8], are considered to be very promising alternative materials owning to their intrinsic high specific capacity [9]. Among these materials, NaCl-type Li_2SnO_3 attracts more attention for its high reversible capacity [10]. However, as Sn-based materials, Li_2SnO_3 suffers from poor cycling performance due to the large specific volume changes and nanoparticle aggregation during Li insertion/extraction processes [11–13]. Several forms of supporting materials have been attempted, such as amorphous carbons [14–16], polyaniline, polypyrrole [17, 18], graphene [19–21], and carbon nanotubes [22]. It shows that doping carbon-based materials may be an effective way to prevent the severe pulverization of Sn-based materials and finally achieve satisfactory electrochemical performances for lithium-ion batteries. The carbon matrix can hinder original particle aggregation, provide continuous long-distance electron transport pathway, support numerous active sites for charge-transfer reactions, and eliminate the need for binding or conducting additive [23].

Bamboo charcoal (BC) is a new class of porous carbonaceous materials. It has been widely used as a contaminant sorbent, because it is cost-effective, renewable, and environmentally friendly [24]. BC can be produced from the widespread moso bamboo plants in China, exhibiting fast-growing speed and short growth period. The bamboo and bamboo residues can be transformed to BC at a high temperature under nitrogen atmosphere, which is a mature

Y. Zhao · Y. Huang (✉) · Q. Wang · W. Zhang · K. Wang · M. Zong
Department of Applied Chemistry and The Key Laboratory of Space Applied Physics and Chemistry, Ministry of Education, School of Science, Northwestern Polytechnical University, Xi'an 710072, People's Republic of China
e-mail: yingh@nwpu.edu.cn

Y. Zhao
e-mail: zhaoyang890@163.com

technology used in China [25]. The structure of BC primarily consists of porous network and surface functional groups, which provide spaces to load nanoparticles on the surfaces [26, 27]. The porous structure and large surface area could limit the volume expansion of the Sn-based materials. Meanwhile, as a kind of carbon material, BC can also be a potential anode electrode for lithium-ion battery. But the Li-storage performances of BC have not been deeply researched.

In this work, first we studied the Li-storage performances of BC. Then the BC/Li_2SnO_3 composites were synthesized by a modified sol–gel method. In this way, Li_2SnO_3 particles are loaded on the surface of BC and some of them enter into its hole. As a result, the as-prepared BC/Li_2SnO_3 composites may show synergistic properties and superior electrochemical performance than BC and Li_2SnO_3.

2 Experimental Procedure

2.1 Sample preparation

The BC was provided by Jiangxi Zhushan Blue Sky bamboo fiber Co., Ltd. (Jiangxi, China). Li_2SnO_3 was synthesized and then loaded onto the BC via a modified sol–gel process [10]. 0.05 mol of $SnCl_4{\cdot}5H_2O$ was first dissolved in 450 ml ultrapure water and then 0.3 mol of ethylene glycol and 0.2 mol anhydrous citric acid were subsequently dissolved in this solution at 50 °C for 1 h. In addition, 0.05 mol of Li_2CO_3 was added into it. Then the mixture was stirred at 90 °C to form sol. When most of the water evaporated, the BC was soaked into the sol for 1 h and then was dried in the drying oven at 180 °C to be a xerogel. Organic matter of the xerogel was rapidly burned at 350 °C and then transferred to a tube furnace in Ar at 400 °C for 5 h. The resulting powder was grinded and sintered at 700 °C in the tube furnace for 5 h at Ar atmosphere.

2.2 Sample characterization

The structure of the prepared samples was characterized by X-ray diffraction analysis (XRD) (Rigaku, model D/max-2500 system at 40 kV and 100 mA of Cu K). The Raman spectra of the composite samples were obtained using a Laser Raman spectrometer (Renishaw Co., England) with a 514-nm radiation. The surface morphology study of the composite was performed by scanning electron microscope (SEM, SuPRA 55, German ZEISS). Thermal analysis of the composite was performed by thermal gravimetric analysis (TGA) (Model Q50, TA, USA) under an air atmosphere, with a heating rate of 20 °C/min, and the temperature range was from 20 to 700 °C.

2.3 Electrochemical measurements

Electrochemical performance was evaluated by a CR2016-type coin cell with a multi-channel current static system land (LAND CT200IA). The anode electrodes were prepared by coating slurries consisting of Li_2SnO_3/BC composite (65 wt%) with acetylene black (15 wt%) and PVDF (20 wt%) as a binder dissolved in 1-methyl-2-pyrrolidinone (NMP) solution on a copper foil. Li foil was used as a counter electrode, and polypropylene (PP) film (Celgard 2400) was used as the separator. The electrolyte was a solution of 1 M LiPF6 in a mixture of ethylene (EC), dimethyl carbonate, and diethyl carbonate (DEC) (1:1:1, v/v/v). Cyclic voltammetry (CV) was performed on a Series G 750^{TM} Redefining Electrochemical Measurement (USA GMARY Co.).

3 Results and discussion

Figure 1a shows the X-ray diffraction (XRD) patterns of BC (H1) and BC/Li_2SnO_3 composites (H2). A broad peak is shown at around 27° characteristic of BC. It can be considered that the graphitization and crystallization process of BC are incomplete. The BC consists of amorphous carbon and graphite microcrystalline due to the low graphitizing. The other four peaks in Fig. 1 (H1) can be attributed to the aluminum substrate. In Fig. 1 (H2), there are two types of diffraction patterns corresponding to Li_2SnO_3 and Sn crystal, respectively. The standard data of Li_2SnO_3 monoclinic crystal structure consist of lattice constants $a = 5.301$, $b = 9.181$, and $c = 10.027$ Å (PDF#31-0761); the data of Sn consist of lattice constants $a = 5.831$, $b = 5.831$, and $c = 3.187$ Å (PDF#04-0673). It is probably that part of the Li_2SnO_3 may be deoxidized by BC in the high-temperature process of the formation of crystals. The rest of Sn particles may be formed directly by sintering incompletely complexed Tin slat under Ar atmosphere.

Figure 1b presents the Raman spectra of BC (H1) and BC/Li_2SnO_3 composites (H2). The peak at about 1592 cm^{-1} (G band) is related to the vibration of sp2-bonded carbon atoms in a 2-dimensional hexagonal lattice, while the 1334 cm^{-1} peak (D band) can be related to the defects and disorder in the hexagonal graphitic layers [28]. H1 shows that the BC consists of amorphous carbon and graphite microcrystalline which obtain a unanimous conclusion with the XRD analysis. It is obviously shown that the structure of BC is not greatly affected after loading of Li_2SnO_3.

Figure 1c shows the TGA analysis of Li_2SnO_3 and BC/Li_2SnO_3 composites. In the TGA curve of BC/Li_2SnO_3 composites, an abrupt weight loss occurs from the room temperature to 100 °C, indicating the evaporation of water

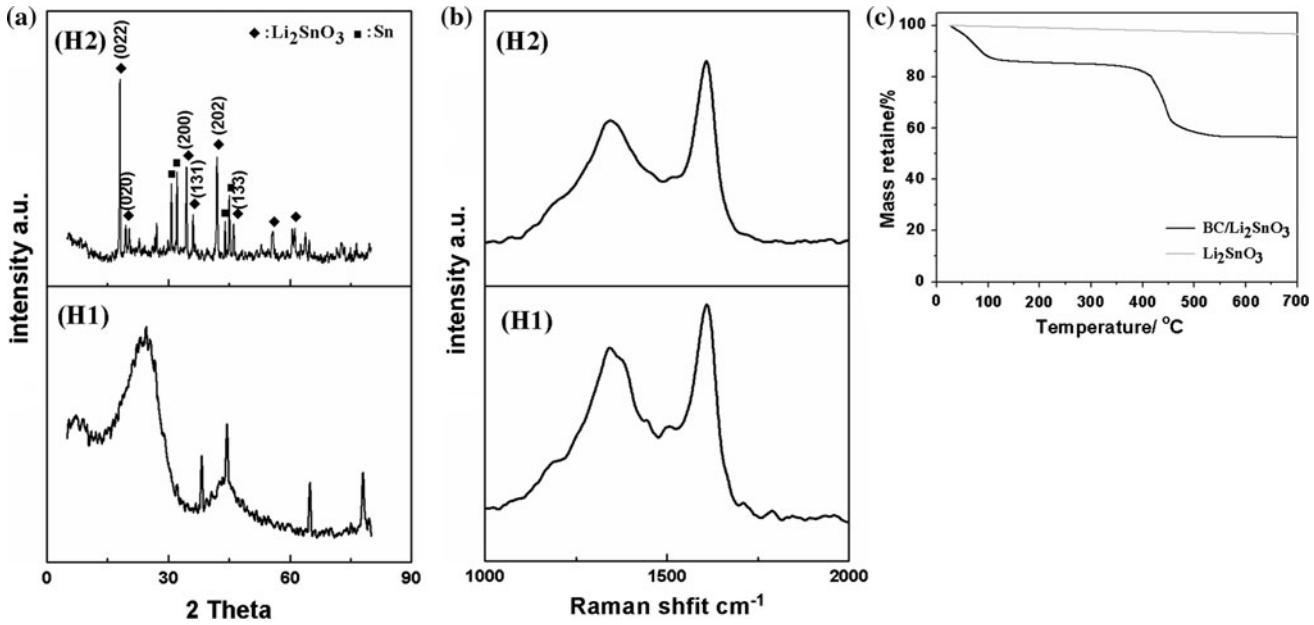

Fig. 1 XRD patterns **a** of BC (H1, BC) and BC/Li_2SnO_3 composites (H2); Raman spectra, **b** of BC (H1) and BC/Li_2SnO_3 composites (H2); TGA curves of Li_2SnO_3 and BC/Li_2SnO_3 composites

in the samples; the weight loss from 400 to 500 °C may be contributed by the oxidation and decomposition of BC in air. Therefore, compared with the TGA curve of Li_2SnO_3, the change in weight before and after the oxidation of BC can be transformed into the change in amount of carbon in the materials. The results show that the mass fraction of BC in the BC/Li_2SnO_3 composites is about 27 wt%.

The SEM images of BC are shown in Fig. 2a, b. There are many micro holes in the BC. The pore sizes of BC are about 1–10 μm. Figure 2b is the sectional view of BC. From the image, the holes are also apparent. These micro holes can provide large growing spaces for Li_2SnO_3. The rest of the images (Fig. 3c–f) are the figures of BC/Li_2SnO_3 composites. From Fig. 3c, e it is obviously shown that part of Li_2SnO_3 coated on the surface of the BC; others are entered into the holes of the BC according to the detail (Fig. 3d, f). The BC is filled with the Li_2SnO_3. These porous structures may limit the volume expansion of the Li_2SnO_3.

The lithium storage capacity and cyclability of as anode in lithium-ion cells were determined via galvanostatic charge/discharge cycling. Fig. 3a, b shows the charge/discharge profiles of BC and BC/Li_2SnO_3 composites electrode in the first and second cycles, respectively. In the first cycle, the composites deliver a lithium insertion capacity of 1688.6 mAh g^{-1} and a reversible charging capacity of 845.5 mAh g^{-1}. The first discharge and charge capacity of the BC are 828.75 and 319.6 mAh g^{-1}. The irreversible discharge capacities after the first cycle for BC has gone away due to severe side reaction with solid electrolyte interphase (SEI) film; there is an additional capacity loss for the composites with the severe side reaction with the electrolyte forming Li_2O. The reaction between Li_2SnO_3 and Li^+ can be described as [19].

$$Li_2SnO_3 + 4Li \rightleftarrows 3Li_2O + Sn \quad (1)$$

$$Sn + xLi \rightleftarrows Li_xSn \quad (x \leq 4.4) \quad (2)$$

To evaluate the rate performance of the BC and BC/Li_2SnO_3 composites, the charge/discharge measurements were carried out at various current densities in Fig. 4a, b. At a current density of 60 mA g^{-1}, the discharge (charge) capacities of BC and BC/Li_2SnO_3 composites could remain about 280.6 mAh g^{-1} (280.1 mAh g^{-1}) and 616.5 mAh g^{-1} (613.0 mAh g^{-1}) up to 50 cycles, respectively. When increasing the current density to 120, 180, 300, and 600 mA g^{-1}, the BC/Li_2SnO_3 composites still could deliver a discharge (charge) capacity of 582 (567.5), 529.4 (520.5), 435.2 (431.5), and 313.2 (308.8) mAh g^{-1} up to 50 cycles, respectively. Despite the large declination capacity of the composite declined largely at high rates, the composite still has an excellent cycling performance, indicating that the BC adding is effective. The capacity of the composites at high rates is still higher than Li_2SnO_3. In Fig. 4b, the capacities for BC at the different rates are shown. As the commercial carbon material, the Li-storage performance of BC at high rates is not very satisfactory.

The galvanostatic charge/discharge cycling results are shown in Fig. 5. The Li_2SnO_3 shows a reversible specific capacity of around 956.3 mAh g^{-1} at a current density of

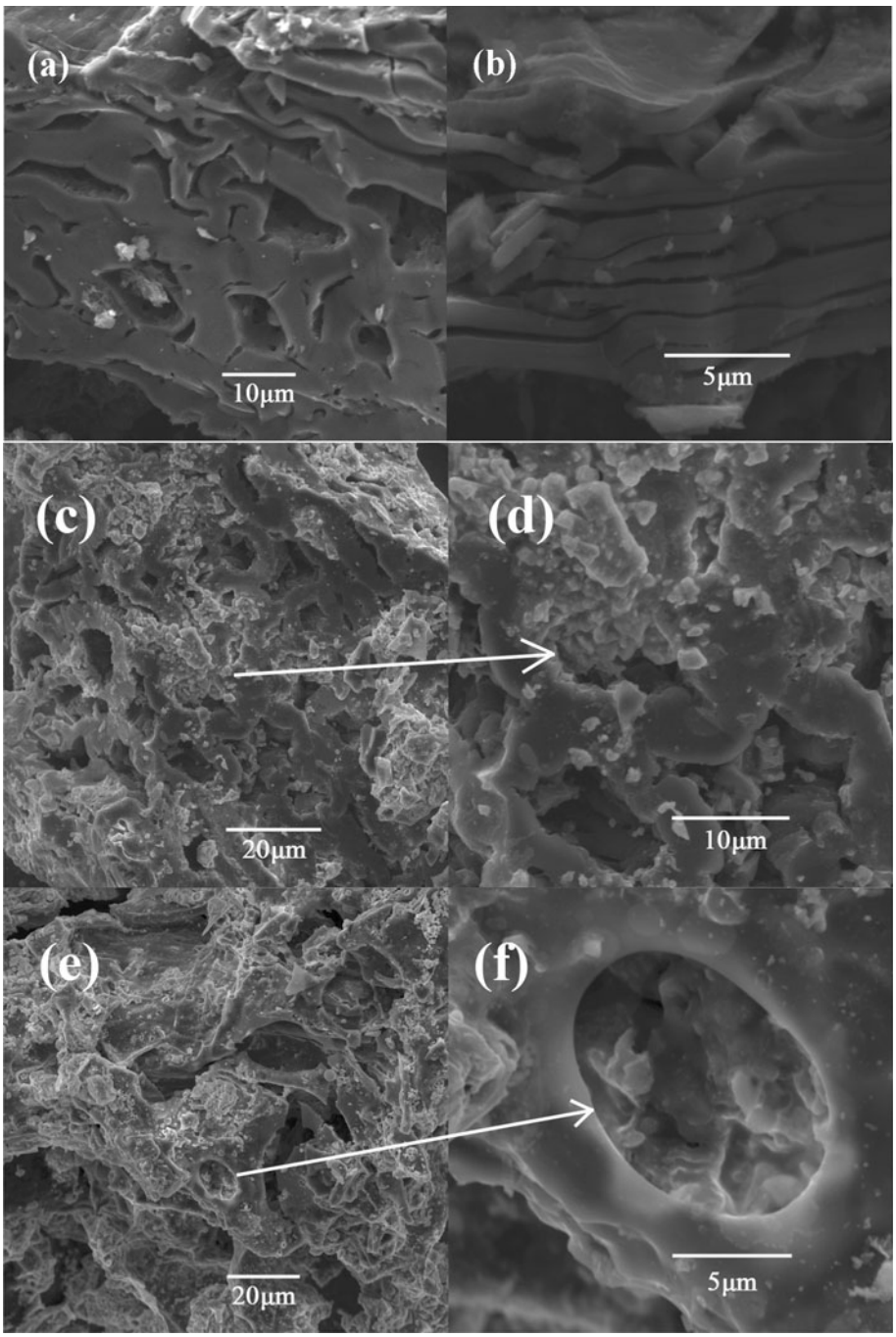

Fig. 2 SEM images of BC (**a**, **b**) and BC/Li_2SnO_3 composites (**c**–**f**)

60 mA g^{-1}. However, the capacity drops dramatically to about 202 mAh g^{-1} at the 30th cycle. The reversible specific capacity of BC is 319.6 mAh g^{-1}. The capacity has gradually attenuated to 280.6 mAh g^{-1} at the 50th cycle. The BC/Li_2SnO_3 shows a good cycle performance and the discharge and charge capacities are 616.5 and 613.0 mAh g^{-1} at the 50th cycle. It can be obviously seen that the capacities of the composites have slowly decreased before the 30 cycles and stabilized after 30 cycles. Beginning with the third cycle, the coulombic efficiency has been stabilized and approaches 95 % at the 50th cycle. The results indicate that the structure of the composites show synergistic properties. In this way, Li_2SnO_3 and BC are effective synergy. The porous structure of BC may buffer a large volume change of Li_2SnO_3 during Li^+ insertion/extraction and cracking of the composite electrode, resulting in an enhanced cycling performance. Comparing with our previous studies, the Li-storage performances of BC/Li_2SnO_3 composites is better than the properties of C/Li_2SnO_3 composites [14, 15], PANI/

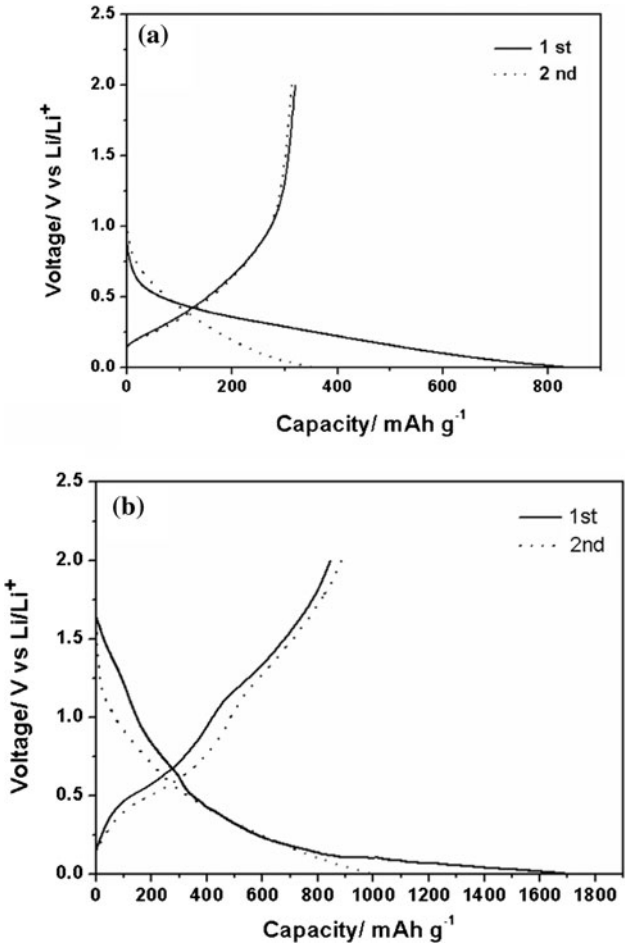

Fig. 3 The first and second cycle charge–discharge voltage profiles for BC (**a**) and BC/Li_2SnO_3 composites (**b**) at current density of 60 mA g^{-1} between 0.01 and 2.0 V

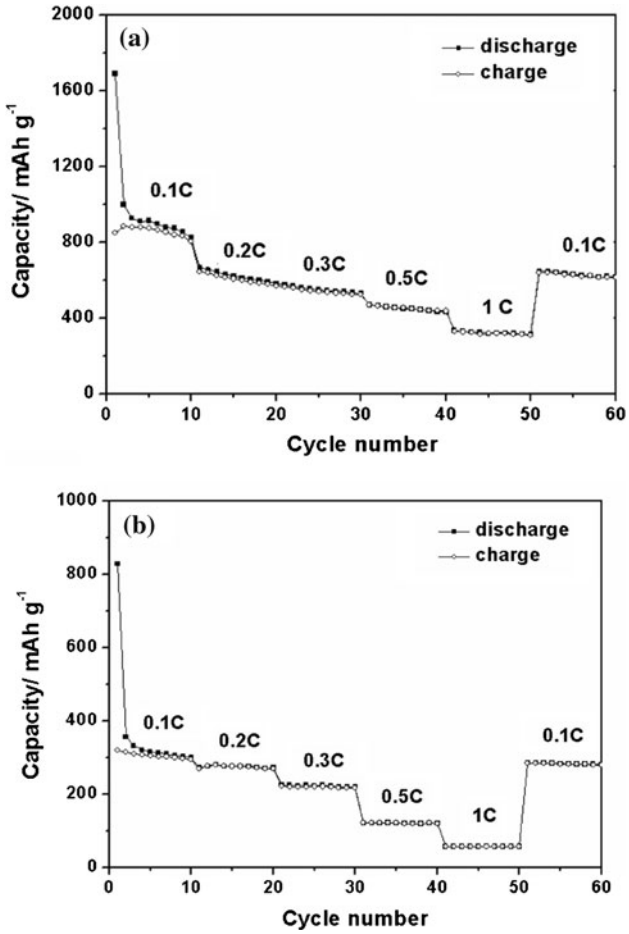

Fig. 4 Cycling performance of BC/Li_2SnO_3 composites (**a**) and BC (**b**) at various charge–discharge current densities between 0.01 and 2.0 V

Li_2SnO_3 composites [17], and graphene/Li_2SnO_3 composites [29].

The electrochemical reactivity of the composites as anode in lithium-ion battery was evaluated by CV. Figure 6a, b shows the CV curves of BC and BC/Li_2SnO_3. The CV curves of BC are in Fig. 6a. In the first cycle of BC, there is a cathodic peak at 0.5 V, which can be attributed to the formation of the solid electrolyte interphase (SEI) layer. This peak disappears in the next cycles. From the second to the fifth cycle, there is a wide oxidation peak at 0.6 V and a reduction peak at 0.2 V. The two peaks can be considered as the intercalation/deintercalation of Li^+ in BC. In the 50th cycle, the oxidation/reduction peaks are still existence, but distinct. It shows that the electrodes are inevitably destroyed during the long cycles. Figure 6b shows the CV curves of BC/Li_2SnO_3. The major oxidation/reduction peaks are still at about 0.6 and 0.2 V. The anodic peak at 0.2 V corresponds to lithium insertion with BC and the alloying of Li_xSn; the cathodic peak at 0.6 V can be assigned to the extraction of lithium from BC and de-

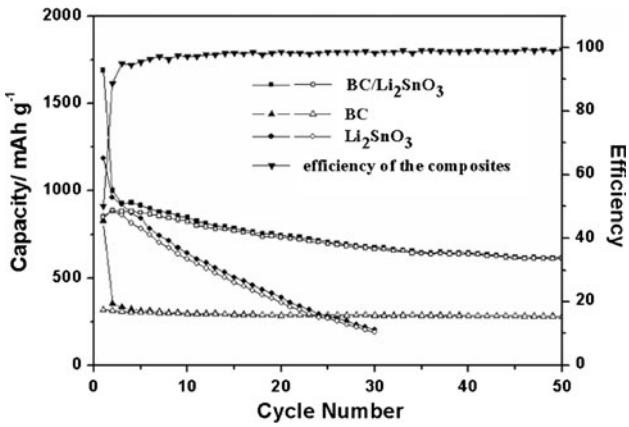

Fig. 5 Cycling performances of Li_2SnO_3, BC, and BC/Li_2SnO_3 composites at current density of 60 mA g between 0.01 and 2.0 V

alloying of Li_xSn [19]. The weak cathodic peak at 1.25 V and the similar anodic peak at 0.8 V may be the partly reversible reaction of Sn and Li_2O [30].

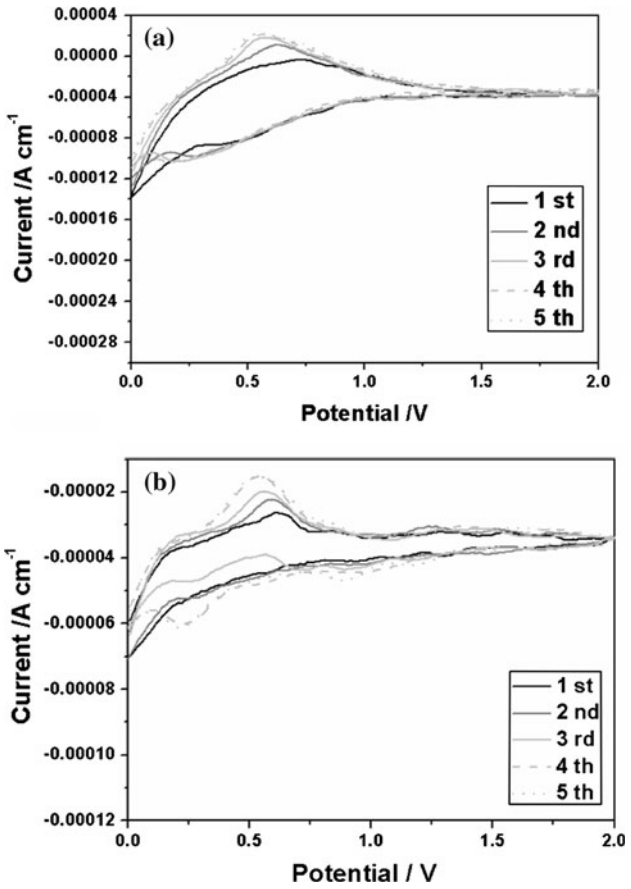

Fig. 6 The cyclic voltammetry of BC (**a**) and BC/Li_2SnO_3 composites (**b**) between 0.01 and 2.5 V at a scan rate of 0.2 mV s^{-1}

In the CV curves of both BC and BC/Li_2SnO_3 composites, the peaks of the initial scans are not well-defined which may be due to the formation of nano Sn in the highly complex matrix of BC or BC/Li_2SnO_3 composites. Lithium ion is difficult to pass through the surrounding matrix to reach the Sn, which may have a distribution of diffusion lengths and corresponding energies. When the increasing critical value of Sn and balanced alloy/de-alloying reactions are achieved, the position of the peaks are not expected to vary.

4 Summary

The BC/Li_2SnO_3 composites were prepared by a sol–gel technique. When tested for lithium storage, the BC/Li_2SnO_3 showed significantly improved cycling performance compared to the Li_2SnO_3 and BC. A capacity of 616.5 mAh g^{-1} can be retained after 50 cycles at the current density of 60 mA g^{-1}. This strategy, with the BC constituting a perfectly supported structure, was demonstrated to be an effective way to improve the cycling performance of anode materials for lithium-ion batteries.

Acknowledgments This work was supported by the Spaceflight Foundation of the People's Republic of China under Grant no. N8XW0002. This work was supported by the Graduate Starting Seed Fund of Northwestern Polytechnical University no. Z2013146.

References

1. Wu YP, Jiang C, Wu C, Holze R (2003) Solid State Ion 156:283–290
2. Sharma Y, Sharma N, Rao GVS, Chowdari BVR (2009) J Power Sources 192:627–635
3. Sharma N, Shaju KM, Rao GVS, Chowdari BVR (2002) Electrochem Commun 4:4947–4952
4. Connor PA, Irvine JTS (2001) J Power Sources 97:223–225
5. Huang F, Yuan ZY, Zhan H, Zhou YH, Sun JT (2003) Mater Lett 57:3341–3345
6. Kim MG, Sim S, Cho J (2010) Adv Mater 22:5154–5158
7. Yang R, Huang J, Zhao W, Lai WZ, Zhang XZ, Zheng J, Li XG (2010) J Power Sources 195:6811–6816
8. Yin XM, Li CC, Zhang M, Hao QY, Liu S, Chen LB, Wang TH (2010) J Phys Chem C 114:8084–8088
9. Wang YX, Huang L, Chang YQ, Ke FS, Li JT, Sun SG (2010) Electrochem Commun 12:1226–1229
10. Zhang DW, Zhang SQ, Jin Y, Yi TH, Xie S, Chen CH (2006) J Alloy Compd 415:229–233
11. Li QY, Hu SJ, Wang HQ, Wang FP, Zhong XX, Wang XY (2009) Electrochim Acta 54:5884–5888
12. Zhu XJ, Guo ZP, Zhang P, Du GD, Poh CK, Chen ZX, Li S, Liu HK (2010) Electrochim Acta 55:4982–4986
13. Aifantis KE, Brutti S, Hackney SA, Sarakonsri T, Scrosatie B (2010) Electrochim Acta 55:5071–5076
14. Wang QF, Huang Y, Miao J, Zhao Y, Wang Y (2012) Mater Lett 71:66–69
15. Wang QF, Huang Y, Miao J, Zhao Y, Wang Y (2012) Appl Surf Sci 258:6923–6929
16. Yuan WS, Tian YW, Liu GQ (2010) J Alloy Compd 506:683–687
17. Wang QF, Huang Y, Miao J, Zhao Y, Wang Y (2012) Appl Surf Sci 258:9896–9901
18. Yuan L, Wang J, Chew SY, Chen J, Guo ZP, Zhao L, Konstantinov K, Liu HK (2007) J Power Sources 174:1183–1187
19. Zhao Y, Huang Y, Wang QF, Wang XY, Zong M (2013) Ceram Int 39:1741–1747
20. Lian PC, Zhu XF, Liang SZ (2010) Electrochim Acta 55:3909–3914
21. Zhao B, Zhang GH, Song JS (2011) Electrochim Acta 56:7340–7346
22. Fu YB, Ma RB, Shu Y, Cao Z, Ma XH (2009) Mater Lett 63:1946–1948
23. Yu YH, Yang Q, Teng DH, Yang XP, Ryu SK (2010) Electrochem Commun 12:1187–1190
24. Tan ZQ, Sun LS, Xiang J, Zeng HC, Liu ZH, Hu S, Qiu JR (2012) Carbon 50:362–371
25. Liao P, Ismael ZM, Zhang WB, Yuan SH, Tong M, Wang K, Bao JG (2012) Chem Eng J 195–196:339–346
26. Liao P, Yuan SH, Zhang WB, Tong M, Wang K (2012) J Colloid Interface Sci 382:74–81
27. Yang FC, Wu KH, Huang JW, Horng DN, Liang CF, Hu MK (2012) Mater Sci Eng, C 32:1062–1067
28. Zhang CF, Peng X, Guo ZP, Cai CB, Chen ZX, Wexler D (2012) Carbon 50:1897–1903
29. Zhao Y, Huang Y, Wang QF, Wang XY, Zong M, Wu HW, Zhang W (2012) Electron Mat Lett. doi:10.1007/s13391-012-2182-z
30. Courtney IA, Dahn JR (1997) J Electrochem Soc 144:2943–2948